Intermolecular Forces in Phase-Change Heat Transfer: *1998 Kern Award Review*

Peter C. Wayner, Jr.
The Isermann Dept. of Chemical Engineering, Rensselaer Polytechnic Institute, Troy, NY 12180

The variation of long-range intermolecular forces near interfaces profoundly affects the performance of change-of-phase heat exchangers. Starting with the fundamental electromagnetic force between molecules (dielectric properties), the effects of shape (Kelvin effect), temperature (Clapeyron effect) and concentration on the heat-transfer characteristics of thin films and larger systems are reviewed and connected. A judicious selection of literature gives a consistent set of models of particular use in heat transfer. Examples of experimental verification of these interfacial models in this rapidly developing field are also presented.

Introduction

Experimental observations and theoretical simulations of the effects of long-range intermolecular forces have demonstrated that the properties of small liquid systems (such as an evaporating drop) deviate from those of a bulk liquid. Deviations also occur near the junction of a liquid film with a substrate. Still additional deviations occur as the thickness of a thin liquid film decreases (such as near the "contact line" where the liquid-vapor interface intercepts the "substrate"). These regions have received extensive study because of their fundamental importance in nature. Herein, this broad literature is reviewed and connected for the purpose of demonstrating its efficacy in modeling change-of-phase heat transfer (such as boiling, heat pipes, grooved evaporators and condensers, rewetting of heated surfaces, and so on). An evaluation of the literature leads us to the conclusion that it is possible to start with two of the four fundamental forces of nature (gravity and electromagnetic (intermolecular)) and obtain the effects of shape (thickness and curvature), concentration, and temperature on the interfacial heat-transfer coefficient and stability of a thin liquid film. This basic understanding has led to important developments in heat-transfer systems.

There is an extremely rich literature concerning equilibrium and nonequilibrium curved liquid films. Therefore, judicious choices are made so that a coherent and consistent understanding of the phenomena of particular use to change-of-phase heat transfer can be discussed. For example, although computational molecular dynamics is extremely useful in analyzing the dynamics of molecules in small systems (for example, see the review by Koplik (1995)), additional development of this field to emphasize interfacial mass transfer is still needed to have an impact on change-of-phase heat-transfer systems. The gradient theory of fluid microstructures is not covered for the same reason (for related material see, for example, the Rowlinson (1979) translation of van der Waals, Davis and Scriven (1981), and Evans et al. (1986). Instead, models based on classical interfacial kinetic theory, quasi-thermodynamics, and continuum concepts are used to simulate the area averaged results that are experimentally observed. However, additional simulation at the molecular level will be needed as systems become smaller and optimized. In essence, the literature on the effect of a nonuniform thin liquid film with shape dependent properties on phase-change heat transfer is reviewed and connected. There have been experimental evaluations of the applicability of the Kelvin equation to highly curved interfaces. For example, Fisher and Israelachvili (1981) demonstrated the validity of the Kelvin equation with systems as small as 4 nm. Use of the bulk viscosity in extremely small thicknesses is still open to question. For example, conflicting results have been presented by Klein and Kumacheva (1995) and Knudstrup et al. (1995). Although roughness can have an additional effect in some cases, roughness greater than that at approximately the molecular level is not addressed. Concerns about using continuum models with ultra-thin films are partially alleviated by averaging over a sufficiently large surface area and time so

that the theoretical results can be experimentally evaluated for confirmation. Confirmed results can then be used for engineering designs.

Since a liquid is deformable, the shape of a liquid film is a function of the three-dimensional (3-D) intermolecular force field. Therefore, the transport processes in a thin film are a function of the liquid-solid system, temperature, concentration, and the shape which is a measure of the varying internal pressure (intermolecular force) field. The optical measurement of shape gives the otherwise difficult measurement of relative pressure in small systems. Two powerful optical techniques based on reflectivity to measure the change in the thin film profile (intermolecular force profile) with heat transfer are discussed herein: image analyzing interferometry (IAI) (DasGupta et al., 1995) and ellipsometry (Kim and Wayner, 1996). Other optical techniques are discussed by Oron et al. (1997).

As outlined in many recent texts, intermolecular and surfaces forces are the result of the electronic structure of atoms and molecules (see, for example, Israelachvili, 1992). At equilibrium, these forces cause the adhesion of one substance to another, the cohesion in bulk liquids, the free energy associated with interfaces, and the liquid-vapor phase distribution in a closed system. An early example of the effect of dielectric properties on change-of-phase heat transfer is given by Wayner (1978). The many noncovalent intermolecular interactions can be broadly classified as follows: (1) electrodynamic Lifshitz-van der Waals (LW) forces (comprising the sum of the London dispersion interaction between two apolar molecules or atoms; the Debye induction interaction and the Keesom orientation interaction); (2) polar forces (hydrogen bonding and Lewis acid-base interactions); and (3) purely electrostatic forces. The London dispersion forces are always present and control transport processes in very thin films with apolar systems. These dispersion forces are long-range forces, vary inversely with the film thickness raised to a power, and can be effective over large distances: from approximately 100 nm, at which an extremely small change from the bulk vapor pressure over a thin liquid film occurs, down to interatomic spacing ($\approx$ 0.2 nm) where the vapor pressure of an adsorbed monolayer can be extremely small. As described by the adsorption isotherm, the thickness of an adsorbed film is a function of the surrounding vapor pressure and substrate temperature. Herein, completely wetting apolar systems will be used as examples because, with simple systems, the van der Waals intermolecular force field can be easily modeled and experimentally studied. Using the insights thereby gained, these concepts can be extended to include more complicated systems.

The material presented in this article covers the details of only a very small portion of the rapidly expanding field of phase change in thin liquid films. There are numerous topics like condensation, two-phase flow, Marangoni flows, and stability that are not emphasized. To obtain additional background information in these areas, the following recent books and reviews are suggested: for a further description of intermolecular forces in thin liquid films (Israelachvili, 1992); for a description of aqueous thin films (van Oss, 1994); for a general description of phase change phenomena (Carey, 1992); for a review of the dynamics and tendency toward rupture of thin liquid films (Bankoff, 1990, 1994; Khanna et al., 1996; Oron et al., 1997); for a recent discussion of the equilibrium and dynamics of evaporating and condensing thin film domains (Sharma, 1998); for additional insights on the modeling of the details of the contact line region (Mitrovic, 1998; Morris, 1997, 1999); for Marangoni flow (see Wayner et al., 1985; Parks and Wayner, 1987; Hallinan et al., 1994; Swanson and Peterson, 1995; Oron et al., 1997); for an extensive discussion of heat pipes (Faghri, 1995).

For a specific example, we start with the description of a constrained vapor bubble (CVB) heat exchanger with transparent quartz walls which embodies many of the concepts that will be subsequently discussed. The CVB, which is presented in Figure 1 for a nonisothermal microgravity environment, has various thin film regions that are of both basic and applied interest. It is formed by underfilling an evacuated small container with liquid. For a completely wetting system at equilibrium, liquid will coat all the walls of the container. For a finite contact angle system, some of the walls can have only an extremely small amount of adsorbed vapor, which changes the substrate properties. Liquid will fill a portion of the corners in both cases. Since the solid walls constrain the shape of the vapor bubble and, therefore, the equilibrium liquid film, the intermolecular force field in the thin liquid film is different from that in a bulk liquid. Both equilibrium, with a uniform temperature field, and nonequilibrium $T_2 > T_1$ studies have been made using the CVB (see, for example, DasGupta et al., 1995; Karthikeyan et al., 1998). Although the thermal conductivity of quartz is small, transparent walls remove the uncertainty concerning liquid shape and are highly desirable in basic research. When heat is supplied at one end and removed at the other end, the effective thermal conductivity due to the evaporation/condensation process can be orders of magnitude greater than that of copper. Vapor flows to the cold end and liquid flows to the hot end due to the shape-dependent intermolecular force gradient. As presented for a relatively large width ($\approx$ 3 mm), the cross-sectional area for vapor flow is much larger than that for liquid flow. As a result, the pressure in the vapor space is nearly

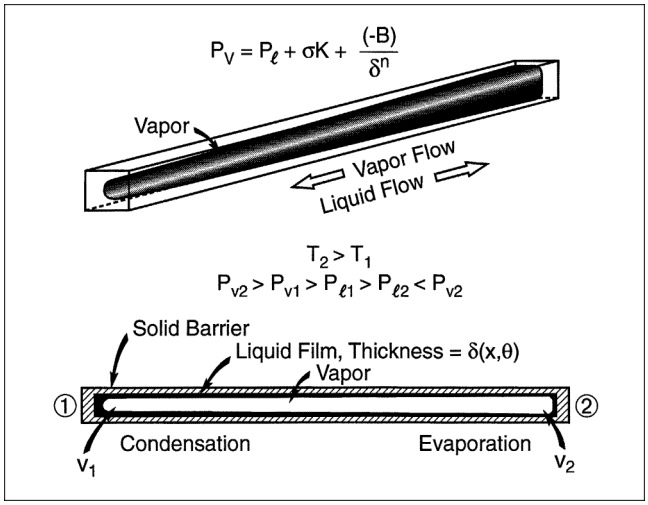

Figure 1. Constrained vapor bubble concept for a completely wetting system in a microgravity field with heat in at End 2 and heat out at End 1.

constant even with high imposed heat fluxes. In this case, the high interfacial heat-transfer coefficient keeps the liquid-vapor interface nearly isothermal, except where the film is extremely thin. In the ultrathin film region where deviations in the intermolecular force field control the transport processes, large interfacial temperature gradients are sustainable. When sufficiently stressed, dry regions with contact lines occur. At the other extreme, the isothermal system is well suited to the study of interfacial thermodynamics. Before discussing the details, the genesis of this particular field of interfacial heat transfer in thin liquid films and examples of a few recent applications will be presented in the next paragraph as an introduction.

In 1965, Derjaguin et al. demonstrated that liquid flow in a thin film on the walls of a capillary tube can enhance by several times the rate of evaporation of moisture from capillaries. The liquid flow, due to long-range intermolecular forces, was analyzed using the disjoining pressure concept for the pressure gradient in the thin liquid film. In 1972, Potash and Wayner analyzed evaporation from a 2-D extended meniscus in which the pressure gradient for liquid flow was due to both capillarity and disjoining pressure. The presence of an adsorbed superheated thin film gave a smooth transition between evaporating and nonevaporating portions of the extended meniscus. The variation of heat flux and local "apparent contact angle" with thickness was calculated as a function of the average heat flow rate. These concepts are of obvious importance to the simpler device presented in Figure 1 and the more complicated systems presented in Figures 2 and 3. In 1973, Raiff and Wayner experimentally and theoretically studied the porous flow control element design presented in Figure 3 which foreshadowed two heat pipe designs: the inverted meniscus heat pipe and the loop heat pipe. In 1984, Cotter used these concepts in proposing a micro heat pipe with a triangular cross-section and side width between 10 and 500 μm. The micro heat pipe has been extensively studied: for example, by Ha and Peterson (1998), Wu and Peterson (1991), and by Khrustalev and Faghri (1993). In 1994, Stephan and Hammer successfully used the interfacial models discussed herein to evaluate the influence of meniscus shape, adhesion forces, interfacial thermal resistance, and wall thermal resistance on nucleate boiling heat transfer using the refrigerant R114/Cu, ($C_2Cl_2F_4$)/Cu, system. For the single bubble and microlayer presented in Figure 2, they calculated realistic temperature and heat flux profiles for boiling heat transfer which agreed with macroscopic experimental results. In an earlier article, Stephan and Busse (1992) successfully used the same type of modeling to analyze the heat-transfer coefficient of grooved evaporator walls. These and many other developments have demonstrated the engineering utility of the material presented herein.

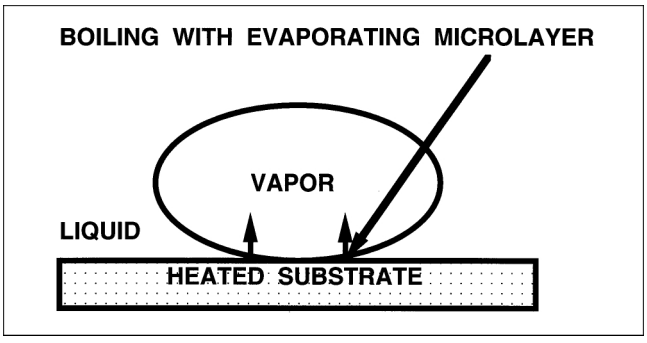

Figure 2. Boiling on a horizontal surface.

Many aspects of the macroscopically observed transport processes in boiling are functions of the interfacial force field in the microscopic extended menisci formed at the base of bubbles. Although the large bulk system is highly turbulent, the thickness of the microlayer region in the oscillating extended meniscus is sufficiently small so that this region can be modeled using laminar principles.

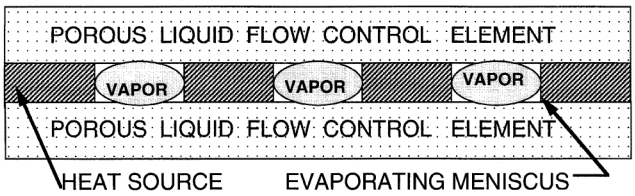

Figure 3. Cross section of meniscus heat pipe concept.

In this case, the vapor exhaust channel perpendicular to the cross-section can be viewed as a steady-state vapor bubble constrained on two sides by a heat source and on two sides by liquid filled porous material. Evaporating extended menisci are formed in the corners at the heat source and supplied with liquid from the porous flow control element by the intermolecular force gradient. At high heat flow rates, the liquid-vapor interface can migrate into the porous element. For a particular example of an application, the heat source could be a microscale electronic device which is cooled by the passive evaporating menisci.

Basic Concepts

Clapeyron effect

Using kinetic theory and the Clausius-Clapeyron equation, an ideal liquid-vapor interfacial heat-transfer coefficient h_{lv}^{id} can be defined by Eq. 1 as the heat-transfer coefficient associated with the surface of a bulk liquid due to a temperature jump at the liquid-vapor interface (see, for example, Carey, 1992; Wayner, 1991). In Eq. 1, T_{lv} is the temperature on the liquid side of a planar liquid-vapor interface and T_v is the temperature on the vapor side. In Eq. 2, Δh_m is the heat of vaporization and the value of the coefficient can be $C = 2$ for simple systems with an accommodation coefficient of unity. For the reference system, T_v is also the equilibrium temperature of a bulk fluid which has an equilibrium vapor pressure of P_v. This interfacial temperature jump gives a "vapor pressure" difference for evaporation and vapor flow away from the interface or for condensation with vapor flow towards the interface. As discussed extensively by Carey (1992), extremely high interfacial heat-transfer coefficients are possible. Additional experimental research on C is reviewed in Maa (1983). Values for the ideal interfacial heat-transfer coefficient for pentane as a function of bulk vapor pressure are given in Figure 4. These large values can be compared with the thermal conductance of the liquid film to determine the thickness at which it becomes important. As an example, for conduction across a liquid pentane film with a thickness of $\delta = 24$ nm, $h = k/\delta = 4.8 \times 10^6$ W/m$^2\cdot$K. This level was selected, because it is equal to the value of h_{lv}^{id} at the atmospheric vapor

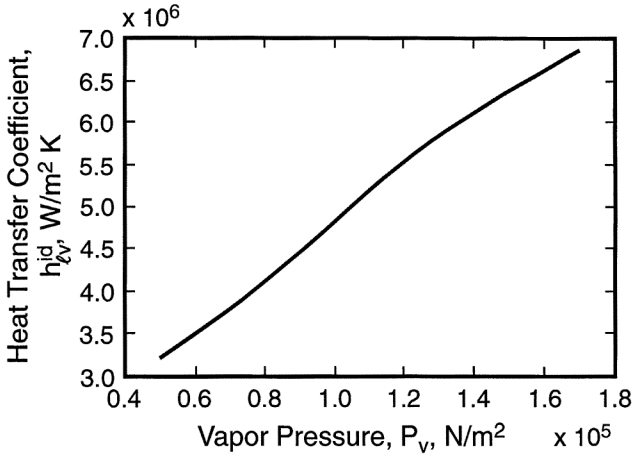

Figure 4. Ideal value of liquid-vapor interfacial heat-transfer coefficients h_{lv}^{id} for pentane as a function of the vapor pressure of the bulk liquid.

pressure of 10^5 N/m^2. We note that significantly larger values of h_{lv}^{id} are attainable with many other systems.

$$q'' = m''^{id}\Delta h_m = h_{lv}^{id}(T_{lv} - T_v) \tag{1}$$

$$h_{lv}^{id} = \left(\frac{C^2 M}{2\pi R T_{lv}}\right)^{0.5} \frac{M P_v \Delta h_m^2}{R T_v T_{lv}} \tag{2}$$

Kelvin effect

Since the values of h_{lv}^{id} and the thermal conductance for thin liquid films are so large, other resistances may limit the heat flux in the contact line region. Three possibilities are the resistance to conduction in the solid, the resistance to fluid flow, and a resistance associated with a change in the vapor pressure of the liquid film due to a change in the intermolecular force field. It is well known that a change in the arrangement of molecules in the interfacial region gives a capillary pressure jump at the interface (such as the interfacial pressure jump associated with the curved meniscus cited above). We find that this shape-dependent change in the intermolecular force field can have a significant, if not controlling, effect on the heat flux in the contact line region.

An example of the variation of chemical potential with film thickness for a thin film is given for a simple spreading case and a simple finite contact angle case in Figure 5a. In the limit $\delta \to 0$, $\mu \to -\infty$ for both cases, but this is not shown for $\theta > 0$ due to the extremely small amount of adsorption. The variation for a complicated system which includes a fluid like water on a polar substrate is given in Figure 5b. This represents an adsorbed ultra-thin film in equilibrium with a thicker film at the "contact line." A discussion of various isotherms is given by Dzyaloskinskii et al. (1961). This early reference is recommended for an understanding of the general theory of van der Waals forces, the DLP (Dzyaloskinskii et al., 1961) thin film continuum model, and the effect of thickness on the vapor pressure.

The enhanced Young-Laplace interfacial pressure jump model represented by Eq. 3 which includes both capillary,

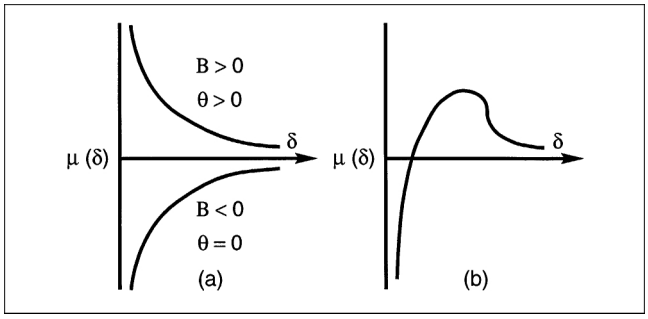

Figure 5. Variation of chemical potential with film thickness (Dzyaloskinskii et al., 1961).

(a) Simple spreading and nonspreading systems; (b) complicated system (such as water on a polar substrate).

σK, and disjoining Π pressure jumps, leads to a change in the vapor pressure over the interface relative to that of a planar interface of a bulk liquid (see, for example, Wayner, 1991). For a completely wetting system, both terms reduce the vapor pressure in the contact line region from that of a bulk liquid. This reduction is given by Eq. 4 in which P_{lv} is the changed vapor pressure of the curved thin film and P_{vr} is the reference vapor pressure. The interface of the bulk fluid is used as an ideal reference where the vapor pressure is the well-known thermodynamic pressure

$$P_v - P_l = \sigma K + \Pi \tag{3}$$

$$RT_{vr} \ln(P_{lv}/P_{vr}) = -V_{lM}(\Pi + \sigma K) \tag{4}$$

{$\Pi = -\tilde{A}/\delta^n$ (for a completely wetting system, $\tilde{A} = A/6\pi < 0$, where A is the fundamental Hamaker constant which is a function of the dielectric properties of the system); for $\delta < 10$ nm, $n = 3$ with $A \approx -1.28 \times 10^{-20}$ J for the pentane/quartz system; for $\delta > 15$ nm, $n = 4$, $\tilde{A} = B \approx -1.1 \times 10^{-29}$ J·m}. In Figure 6, values for the disjoining pressure jump at the interface of a flat pentane film on quartz are given. Assuming only

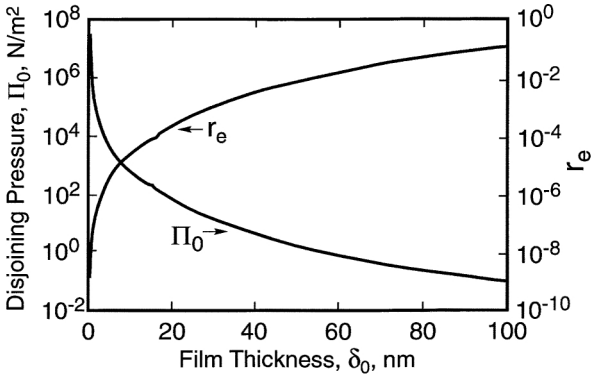

Figure 6. Equilibrium disjoining pressure for a flat film of pentane on quartz Π_o N/m^2 vs. equilibrium film thickness δ_o and the equivalent radius of curvature r_e m for the same pressure jump across a meniscus assuming the absence of disjoining pressure.

capillarity without disjoining pressure for the purpose of discussion, the value of the equivalent radius of curvature for a meniscus is also given for comparison. Large values are obtained as the value of the film thickness approaches that of a monolayer and/or the value of the radius of curvature, $r = 1/K$, becomes very small. We quickly note that both terms should be included in Eq. 3.

A physical understanding of the effect of the interfacial pressure jump on the heat flux can be obtained using the following extended form of Eq. 1, which includes both the Kelvin and Clapeyron effects on the vapor pressure (see, for example, Potash and Wayner, 1972; DasGupta et al., 1994)

$$q'' = m''\Delta h_m = h_{lv}^{\mathrm{id}}(T_{lv} - T_v) + h_{lv}^{kl}(P_l - P_v) \tag{5}$$

$$h_{lv}^{kl} = \left(\frac{C^2 M}{2\pi R T_{lv}}\right)^{0.5} \frac{V_{lM} P_v \Delta h_m}{R T_{lv}} \tag{6}$$

For pentane $T = 293$ K, $h_{lv}^{kl} = 4.25$ (W/m^2)/(N/m^2). For a reduction of heat flux of $q'' = 4.25 \times 10^6$ (W/m^2), $(P_l - P_v) = -10^6$ (N/m^2), for which the radius of curvature would have to be equal to $r = 16$ nm. This large effect can be easily present when fluid flows towards the contact line due to intermolecular suction. For an adsorbed flat film with an equivalent disjoining pressure, the equilibrium thickness of the superheated adsorbed film would be $\delta_o = 0.88$ nm. Therefore, we find that interfacial forces can easily control the heat flux in a superheated adsorbed film. In essence, the Kelvin effect can remove the singularity associated with conduction across a liquid film of vanishing thickness. We also suggest that phase change can remove the singularity usually associated with the "no slip" boundary condition on an "isothermal" or nonisothermal substrate in spreading (Wayner, 1994a,b; Reyes and Wayner, 1996). However, this is usually neglected in current studies on spreading where slip and surface diffusion mechanisms are used to relieve the infinite stress (see, for example, the review by Kistler, 1993). Although the correct model to use at the contact line is unresolved, it seems that both temperature and pressure should be important.

Interfacial free energy and the Hamaker constant

Equations 3–5 demonstrate the importance of surface tension and the Hamaker constant on the interfacial heat-transfer coefficient. To overcome the theoretical difficulties associated with intermolecular forces at interfaces, various useful models have been developed. Gibbs (1961) developed the very successful surface formalism of a 2-D dividing surface: the Gibbs convention. At times, this convention and the resulting interfacial free energy are extremely useful. In many other situations, like transport processes in ultra-thin liquid films, we find it more useful to include the thickness of the thin film which is not easily described within the Gibbs convention. To include thickness, a 3-D model is needed. This requires either the surface excess convention or the film excess convention. Both the Gibbs and the surface excess conventions are used herein, thereby showing the connection between the two conventions. The surface excess convention allows the disjoining pressure concept, which is an effective pressure change due to intermolecular force changes in a planar thin film, to be introduced. A good discussion and comparison of the details of these two conventions are given by deFeijter (1988). It is the first chapter in a recommended book on thin films by Ivanov (1988).

When a liquid drop is placed on a substrate, the resulting system can be classified as either completely spreading, partially spreading, or nonspreading. For complete spreading, the final equilibrium shape is one of a thin uniform film covering the substrate (presuming that the vapor pressure in the surroundings is sufficient to suppress evaporation). Simple diagrams of the completely spreading and partially spreading cases in a gravitational field are presented in Figure 7. The picture of the completely wetting case conceptually represents, for an extremely thin case, a monolayer or, at the other extreme, a much thicker film. For the partially wetting case, a deceptively simple quantitative measure of the complex intermolecular force field in the contact line region is the apparent contact angle θ. The contact angle is defined as the angle between the tangents to the liquid-vapor and liquid-solid interfaces at a point where the film is sufficiently thick so that the transition regions in the interfaces do not overlap. For some cases, like a small drop on a substrate, this definition is still inexact since the observable tangent angle constantly changes. For the nonwetting case, $\theta > 90°$. At this point, it is becoming obvious that mathematical interfaces and apparent contact angles are relatively crude but useful (at times) descriptions of the complex dynamic molecular world at interfaces and contact lines. For example, try to picture the real contact angle in the contact line region of a moving contact line using a molecular dynamic simulation model.

The interfacial free energy can be composed of dispersion (London) d, polar (Keesom) p, induced dipole (Debye) i, electrostatic e, and acid-base interactions AB

$$\sigma = \sigma^d + \sigma^p + \sigma^i + \sigma^e + \sigma^{\mathrm{AB}} \tag{7}$$

The first three terms in this equation are the Lifshitz-van der Waals interactions σ^{LW}. Simple fluids like the alkanes have only LW interactions. Some representative values for the terms in Eq. 9 for polar fluids are given by van Oss (1994). For apolar liquids like the alkanes emphasized below, $\sigma = \sigma_l = \sigma^{\mathrm{LW}}$.

To connect these concepts and the Hamaker constant with experimental observations, we assume (at times) that there is no practical difference between these processes of interfacial formation occurring in a vacuum and an environment saturated with vapor or gas ($\sigma_l \cong \sigma_{lv}$, $\sigma_s \cong \sigma_{sg}$ or σ_{sv}). However,

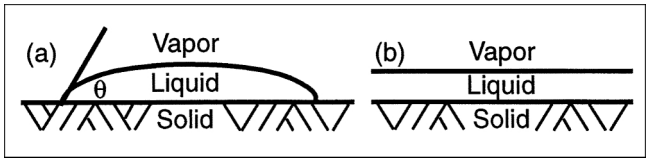

Figure 7. Simple macroscopic views of a liquid film on a solid substrate.

(a) Partially wetting liquid drop; (b) completely wetting liquid film.

it is also important to realize that the interfacial free energy values can, in some cases, be substantially different in laboratory air because of the adsorption of foreign vapor molecules like water and hydrocarbons. At liquid-vapor interfaces, impurities may or may not concentrate at the surface and thereby affect the value of the interfacial free energy. A further complication can arise if the environment has a foreign gas which can adsorb on the liquid substrate and change σ_l to σ_{lg}. Therefore, there are many practical complications when these concepts are used in modeling transport processes. On the other hand, all these additional effects can be experimentally measured and theoretically modeled. As examples, practical experiments on the effect of the environment on the surface tension of stainless steel are discussed by Mantel and Wightman (1994) and a theoretical analysis of the wetting of gold by water is given by Parsegian (1977). The reader will find it necessary to use, as the situation dictates, both practical and ideal concepts to understand and apply the state of the art in surface transport processes. The current trend towards smaller closed devices is a trend towards more ideal systems.

Equation 8 is the Young equation for the contact angle of a liquid on a substrate in its equilibrium vapor environment (see, for example, Wayner, 1982, who also gives a continuum model for the important details of the thickness profile in the transition region using the disjoining pressure concept).

$$\sigma_{lv} \cos \theta = \sigma_{sv} - \sigma_{sl} \tag{8}$$

This can also be written as

$$\sigma_{lv} \cos \theta = \sigma_s - \sigma_{sl} - \pi_e \tag{9}$$

where $\pi_e = \sigma_s - \sigma_{sv}$ is the equilibrium film pressure which accounts for adsorption on the solid substrate (Bangham, 1937).

Hamaker constant (apolar systems)

To relate the interfacial free energies to the dielectric properties of the materials and to use the surface excess convention for thin films, it is necessary to introduce the Hamaker constant (see, for example, Israelachvili, 1992, for additional details). The Hamaker constant A_{ii}, which describes the LW interaction between two bulk flat surfaces in a vacuum separated by the van der Waals contact distance D_s, is, for a liquid

$$A_{ll} = 24\pi D_s^2 \sigma_l \tag{10}$$

The Hamaker constant is defined as

$$A = \pi^2 C \rho_1 \rho_2 \tag{11}$$

where ρ_1 and ρ_2 are the number of atoms per unit volume in the two volumes and C is a coefficient describing the interaction between two atoms. The theoretical value of the separation distance between two semi-infinite slabs when they are in van der Waals contact is $D_s = 1.65 \times 10^{-10}$ m. For two bulk solids and a solid-liquid interface, the comparable equations are

$$A_{ss} = 24\pi D_s^2 \sigma_s, \quad A_{sl} \approx 24\pi D_s^2 \sqrt{\sigma_s \sigma_l} \tag{12}$$

The Hamaker constant between two like bodies is attractive, $A_{ii} > 0$. Exact procedures to obtain the Hamaker constant from the frequency-dependent dielectric functions of the interacting materials using the DLP theory are addressed by Israelachvili (1992). For now, the following *approximate* equation adequately demonstrates the connection between the Hamaker constant and the dielectric constant ϵ, the refractive index in the visible range n_o, and the plasma frequency of the free electron gas ν_e

$$A = \frac{3kT}{4}\left(\frac{\epsilon_o - 1}{\epsilon_o + 1}\right)^2 + \frac{3h\nu_e\left(n_o^2 - 1\right)^2}{16\sqrt{2}\left(n_o^2 + 1\right)^{3/2}} \tag{13}$$

Using Eq. 13, $A_{ll} \approx 3.8 \times 10^{-20}$ J for pentane and $A_{ss} = 6.3 \times 10^{-20}$ J for quartz. Since $A_{ss} > A_{ll}$, this is a completely wetting system. Wayner (1978) used these equations and the combining rules below to evaluate the effect of the London-van der Waals dispersion force on the interline heat flow rate.

In order to discuss surface and adhesion energies, Israelachvili (1992) showed that, apart from the bulk cohesive energy, the additional energy of two planar surfaces separated by the distance δ is

$$E = \frac{A}{12\pi}\left(\frac{1}{D_s^2} - \frac{1}{\delta^2}\right) \tag{14}$$

The interaction energy is

$$E_i = \frac{-A}{12\pi\delta^2} \tag{15}$$

Equation 10 is obtaining by taking $E = 2\sigma_l$ at $\delta \to \infty$. The additional potential energy is removed when the two interfaces are brought into contact. The adhesive pressure in contact F at D_s is

$$F = \left(\frac{\partial E}{\partial \delta}\right)_{\delta = D_s} = \frac{A}{6\pi D_s^3} = \frac{4\sigma_l}{D_s} \tag{16}$$

The intermolecular forces are very large and large energy gradients can occur over very short separations. For two planar octane surfaces in van der Waals contact ($D_s = 0.165$ nm), Eq. 16 gives $\sigma_l = 21.9$ mN/m, whereas the experimental value is $\sigma_l = 21.6$ mN/m) and F is approximately 5,200 atmospheres. For pentane, the experimental value of σ is 14% less than the value given by Eq. 16. There is an extremely large change in the internal pressure due to cohesion and adhesion over a very short distance at the liquid-vapor and liquid-solid interfaces that effects phase change.

For a thin film on a solid, the repulsive force per unit area between the bulk vapor and the bulk solid separated by a liquid film is (for example, see Truong and Wayner, 1987), for the nonretarded regime

$$F(\delta) = \frac{A_{slv}}{6\pi\delta^3} = -\Pi, \quad \delta \lesssim 10 \text{ nm} \tag{17}$$

while for a thicker film (retarded regime using a dispersion constant B),

$$F(\delta) = \frac{B_{slv}}{\delta^4} = -\Pi, \quad \delta \gtrsim 15 \text{ nm} \tag{18}$$

Calculations of the van der Waals interactions between different materials using the DLP theory showed that A_{slv} and B_{slv} are not constant but, depending on conditions, a weak function of film thickness in their respective regimes. Keeping this in mind, we can still obtain approximate equations for effective modeling. Caution is advised, because two sign conventions are used in the literature. The sign convention used herein makes $A_{slv} < 0$ for completely wetting systems and $A_{slv} > 0$ for partially wetting systems. The above equations also give the equivalence between the disjoining pressure concept Π and the dispersion force per unit area. The easiest description of disjoining pressure is given in Figure 8, in which an air/vapor bubble is captured by an inverted cup and pushed down against the bottom surface of the container holding the liquid. If the liquid completely wets the substrate, a film of liquid disjoins the bubble from the substrate even though the pressure in the bubble is greater than the pressure in the liquid. The liquid in this film is under tension. For completely wetting systems, the vapor is disjoined from the solid by the liquid with a force/area, Π.

Some of the approximate combining rules for the Hamaker constant in Eq. 17 are (for example, Israelachvili, 1992)

$$A_{slv} = A_{sv} + A_{ll} - A_{sl} - A_{lv} \tag{19}$$

$$A_{slv} = \left(\sqrt{A_{ss}} - \sqrt{A_{ll}}\right)\left(\sqrt{A_{vv}} - \sqrt{A_{ll}}\right) \tag{20}$$

neglecting cohesion in the vapor gives

$$A_{slv} = A_{ll} - \sqrt{A_{ll} A_{ss}} \tag{21}$$

Using the previous values for the pentane/quartz system, Eq. 21 gives the approximate value $A_{slv} \approx -1.1 \times 10^{-20}$ J. Using Eqs. 10, 12 and 21 gives

$$A_{slv} = 24\pi D_s^2 \left(\sigma_l - \sqrt{\sigma_l \sigma_s}\right) \tag{22}$$

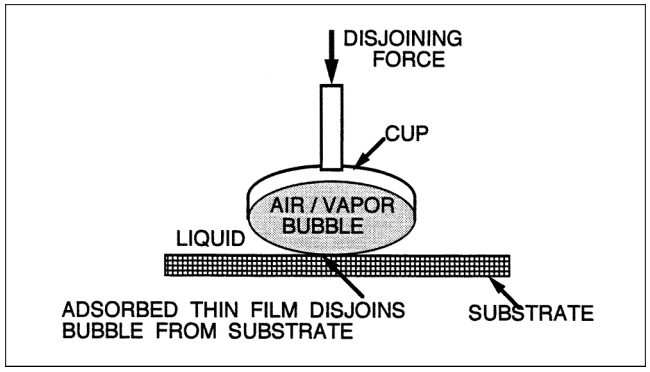

Figure 8. Disjoining pressure concept for completely wetting liquid.

Thin liquid film of adsorbed vapor disjoins the air/vapor bubble from the substrate against which it is being forced.

A completely spreading system is one for which $\sigma_s > \sigma_l$ and $A_{slv} < 0$. This means that, for spreading with a completely wetting system, the liquid-solid intermolecular force field causes the liquid to flow along the surface and thereby separate the solid from the bulk gas-vapor mixture. This also changes the local vapor pressure of the thin film. We note that transport can, of course, occur through both the vapor phase and along the surface. It is very difficult to determine which one predominates at the contact line during spreading.

The following equations have also been developed for apolar systems.

$$\sigma_s^d = \frac{1}{4}\sigma_{lv}(1+\cos\theta)^2, \quad \theta > 0$$

using dispersion force only and $\pi_e = 0$ (23)

Therefore, the dispersion component of the surface tension of a solid can be determined by measuring the contact angle of an apolar liquid on the solid.

For completely wetting fluids, the following equation for the interaction between a solid and vapor separated by a thin liquid film can be obtained

$$\frac{A_{slv}}{12\pi D_s^2} = \sigma_l + \sigma_{sl} - \sigma_s \tag{24}$$

With $\sigma_l \cong \sigma_{lv}$

$$\sigma_s^d = \frac{1}{\sigma_{lv}}\left[\sigma_{lv} - \frac{A_{slv}}{24\pi D_s^2}\right]^2, \quad \theta = 0$$

using dispersion force only (25)

Therefore, the dispersion portion of the interfacial free energy of solids for apolar completely wetting systems can be obtained using the measured value of the Hamaker constant. Since the above equations apply to both wetting and partially wetting systems, Eqs. 21 and 23 can be equated to obtain the following equation for the contact angle in partially wetting systems $A_{slv} > 0$

$$\cos\theta = 1 - \frac{A_{slv}}{12\pi\sigma_l D_s^2}, \quad \pi_e = 0, \quad \theta > 0 \tag{26}$$

There are many additional complications associated with acid-base systems like water (see, for example, van Oss, 1994).

Water/quartz polar system

After reviewing the state of the art of contact angles and surface forces, Churaev (1994) concluded that the theoretical prediction of contact angles is still an unsolved problem. This is particularly true for water as demonstrated by the following discussion of the water/quartz system given by Churaev (1994). We note that we are using a sign convention opposite from that used by Churaev. Thin liquid films are asymmetric systems with liquid-solid and liquid-vapor interfaces, and an additional electrostatic disjoining pressure due to the electri-

cal double layer which can be present. The 3-D disjoining pressure model for a thin liquid film is

$$\Pi(\delta) = \Pi_m(\delta) + \Pi_e(\delta) + \Pi_s(\delta) \tag{27}$$

in which the subscripts m, e, and s refer to the molecular (dispersion), electrostatic, and structural components of the disjoining pressure. The structural forces causing the structural component are short-range forces at the liquid-solid interface.

Frumkin and Deryaguin used the theory of long-range forces to obtain the following relationship between the contact angle and the disjoining pressure

$$\cos\theta = 1 + \frac{1}{\sigma_{lv}}\int_{\delta_\alpha}^{\infty}\Pi(\delta)d\delta = 1 + \frac{G(\delta_\alpha)}{\sigma_{lv}} \tag{28}$$

For $\theta > 0$, $G < 0$ is an excess surface free energy. The characteristic thickness of the adsorbed thin film at $\Pi = 0$ is δ_α. The prediction of the contact angle in polar systems is particularly complicated because, depending on the system, each of the components of the disjoining pressure may be either positive or negative.

As an example of a particular application, Churaev (1994) presented the following equation for estimating the contact angle on *hydrophobic* surfaces when all three components of the disjoining pressure are important

$$\cos\theta = 1 + \frac{1}{\sigma_{lv}}\left\{\frac{-A_{slv}}{12\pi\delta_\alpha^2} - \frac{\epsilon_o(\Psi_1 - \Psi_2)^2}{8\pi\delta_\alpha} + K\lambda\exp\left(-\frac{\delta_\alpha}{\lambda}\right)\right\} \tag{29}$$

where K and λ are parameters, Ψ_1 and Ψ_2 are the surface potentials, δ_α is a film thickness, and ϵ_o is the permittivity of the fluid. Obviously, the equation for the contact angle and its subsequent use in heat transfer becomes very complicated for water.

It is useful to look at the effect of the degree of hydrophilicity on the polymolecular adsorption of water vapor on a quartz surface. In this case, it appears that the short-range forces at the liquid-solid interface can make the film more hydrophilic. Two experimental isotherms by Gee et al. (1990) demonstrated that, with a completely hydroxylated surface (4.6 OH groups per 100 A^2), the system was completely wetting, whereas, using a quartz surface covered with 10% hydroxyl groups, the contact angle was $\theta = 43°$. The hydroxylated surfaces were obtained by using a mild etching solution of 1.5% w/v NH_4HF_2 for 2 h at room temperature. Gee then removed the hydroxyl groups by heating the surface to 1,323 K (which is higher than necessary) to obtain a dehydroxylated surface. Therefore, the contact angle can be varied by varying the number of hydroxyl groups per unit area. Although this might be difficult to achieve, maybe these surfaces of varying hydrophilicity could be sufficiently controlled to produce heat-transfer systems of engineering importance. However, as discussed by Vigil et al. (1994), the description of this classical interface is still unresolved.

Disjoining pressure

We can experimentally obtain the value of the disjoining pressure and the Hamaker constant using the optically measured extended meniscus profile in the CVB and the following set of boundary conditions for Eq. 3 which applies at equilibrium for a constant interfacial pressure jump:

B C 1: For the uniform film thickness portion at the center of a relatively large bubble: $\delta \to \delta_o$, $\Pi \to \Pi_o$, $K \to 0$.

B C 2: For the curved thicker portion of the film: $\Pi \to 0$, $K \to K_\infty$.

Using these two boundary conditions at equilibrium, Eq. 3 gives

$$\sigma K_\infty = -B/\delta_o^4 \quad \text{for } \delta > 15 \text{ nm}$$
$$\sigma K_\infty = -A/6\pi\delta_o^3 \quad \text{for } \delta < 10 \text{ nm} \tag{30}$$

The measured film thickness profile gives K_∞ and δ_o and, therefore, the value of the constant B. As described below, these measurements have been successfully made using the CVB to obtain the value of the Hamaker constant. Earlier references to this field are Derjaguin et al. (1988) and Read and Kitchener (1969). For mass-transfer equilibrium $m'' = 0$, Eq. 5 leads to Eq. 31 for the equilibrium thickness δ_o of a flat adsorbed film as a function of the substrate superheat ΔT. Values for the pentane/quartz system at 293 K are given in Table 1. Of particular significance is the superheat associated with a thickness of approximately a monolayer: $\Delta T = 40$ K is approximately the superheat at the critical heat flux in pool boiling when wetting of the substrate ceases. This will be discussed in a later section.

$$\delta_o^3 = \frac{-\bar{A}T_v}{\rho_{lm}\Delta h_m \Delta T}, \quad \delta_o < 10 \text{ nm} \tag{31}$$

Completely wetting extended meniscus

In Figure 9, a vertical completely wetting extended evaporating meniscus is presented with three regions (Potash and Wayner, 1972; Wayner, 1991): (1) an evaporating intrinsic meniscus, which is defined as that portion where the pressure jump at the interface is described by the conventional equation of capillarity because the film thickness is relatively large (> 100 nm); (2) an evaporating thin film region described by both capillarity and disjoining pressure; (3) an equilibrium flat thin film region. At equilibrium, using thermodynamics for a gravitational field, the connection between the concepts of gravitational pressure drop, capillarity, disjoining pressure,

Table 1. Equilibrium Film Thickness for Pentane on Quartz at 293 K vs. Substrate Superheat Obtained Using Eq. 31 and the Modified Hamaker Constant $\bar{A} = -6.8\times10^{-22}$ J

ΔT, K	δ_o, nm
10^{-5}	44
10^{-2}	4.4
0.1	2.04
1	0.95
10	0.44
40	0.28

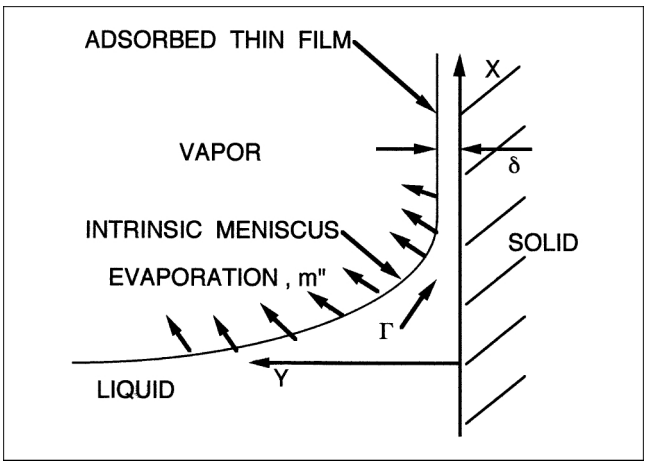

Figure 9. Vertical completely wetting extended evaporating meniscus with a local liquid flow rate of $\Gamma(x)$.

vapor pressure, and adsorption become obvious (Wayner, 1991) and a better understanding of the effect of adsorption due to van der Waals forces is thereby obtained.

Using the above concepts with the lubrication model for laminar flow, Eq. 32 can be obtained for the film thickness profile of a steady-state horizontal evaporating extended meniscus (DasGupta et al., 1994). Although Marangoni effects are not included in this simplified form of the equation, their relative importance has been evaluated by Parks and Wayner (1987), Hallinan et al. (1994), and by Swanson and Peterson (1995). The term ϕ is the dimensionless extended Young-Laplace equation for small slopes which shows the strong influence of surface tension and the Hamaker constant.

$$\frac{1}{3}\frac{d}{d\xi}\left(\eta^3\frac{d\phi}{d\xi}\right)=\frac{1}{1+\kappa\eta}(1+\phi) \tag{32}$$

$$\phi=-\frac{1}{\eta^3}-\epsilon\frac{d^2\eta}{d\xi^2},\quad \eta=\frac{\delta}{\delta_o},\quad \xi=\sqrt{\frac{x^2 v h_{lv}^{\mathrm{id}}\Delta T_o}{-\bar{A}\Delta h_m}}$$

$$\kappa=\frac{h_{lv}^{\mathrm{id}}\delta_o}{k_l},\quad \epsilon=-\frac{\sigma v\delta_o h_{lv}^{kl}}{\Delta h_m\bar{A}}$$

There are many uses for Eq. 32: for example, the righthand side is the dimensionless interfacial heat flux. Examples of theoretical studies of the evaporating meniscus are Potash and Wayner (1972), Kamotani (1978), Holm and Goplen (1979), Moosman and Homsy (1980), Swanson and Herdt (1992), DasGupta et al. (1994), Khrustalev and Faghri (1995), and Morris and Moreno (1997).

Neglecting curvature effects, Eq. 33 for the dimensionless interfacial heat-transfer coefficient can be obtained from the righthand side of Eq. 32 (Wayner et al., 1976). Therefore, we quickly demonstrate that the evaporation rate vanishes when $\delta=\delta_o$, the adsorbed equilibrium thickness, (see Table 1 for values) and reaches 96% of the ideal interfacial evaporation rate when $\delta=3\delta_o$. Using the above cited numbers for the pentane/glass system as an example, mass-transfer equilibrium occurs at $\delta=\delta_o=0.28$ nm for $\Delta T=40$. Whereas, a very large evaporative heat-transfer coefficient (see Figure 4) occurs a short distance away at approximately $\delta=0.84$ nm where adsorption effects essentially vanish. We note that it is still possible to have a lower heat flux because of the effects of capillarity on the vapor pressure and thermal conductive resistances in the liquid and solid. Therefore, we find that very large changes in the force field occur over the distance of approximately a nanometer and that the disjoining pressure concept allows the effects of both temperature and effective pressure in the liquid to be evaluated. A singularity is thereby avoided.

$$\frac{h_{lv}}{h_{lv}^{\mathrm{id}}}=1-\frac{1}{\eta^3}\quad\text{or}\quad h_{lv}=h_{lv}^{\mathrm{id}}\left[1-\left(\frac{\delta_o}{\delta}\right)^3\right] \tag{33}$$

Fluid mixtures

Evaporative flow in an extended evaporating meniscus is a distillation process if a second component is present. Since the contact line region is extremely thin, even a very small amount of a second component in the bulk fluid portion of the system can significantly affect the contact line region. Although some research has been done on this very broad topic, these effects have not been sufficiently studied (see, for example, Wayner et al., 1985; Parks and Wayner, 1987; Huang et al., 1998).

Related Experimental Studies

There is a developing experimental literature that confirms the above modeling: a few examples of this work follow. Using the quartz CVB cell presented in Figure 1, the film profile near the corner of the cell was optically measured at equilibrium using the setup presented in Figure 10. The naturally occurring interference fringes were analyzed using an image analyzing interferometer (IAI) to obtain the shape of

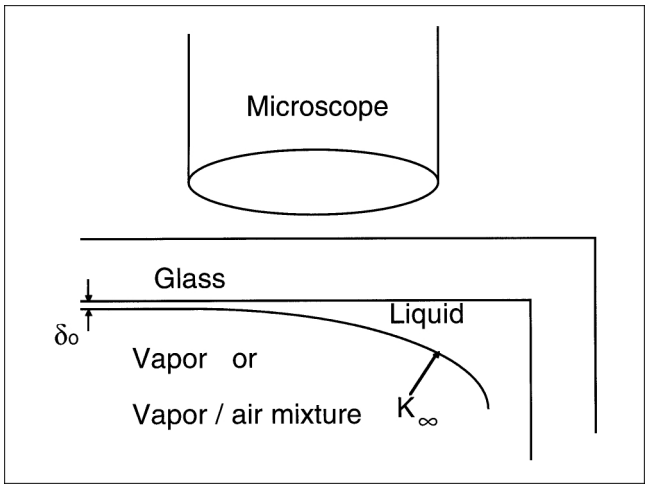

Figure 10. Microscopic view of the meniscus formed in the corner of the CVB using an image analyzing interferometer IAI.

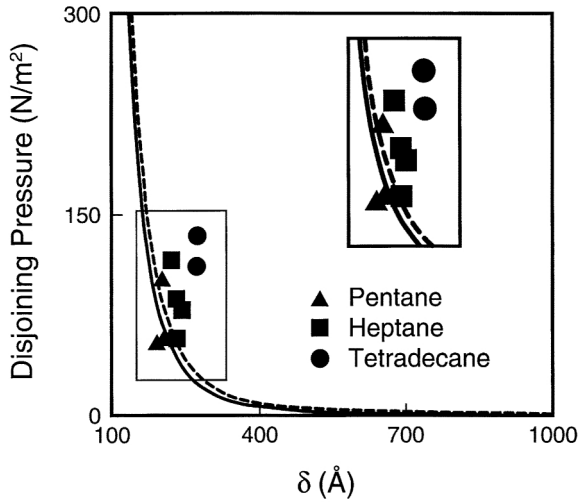

Figure 11. DLP theory for an ideal surface vs. experiments for the adsorption of pentane and heptane on quartz (solid line) and tetradecane on SFL6 (DasGupta et al., 1995).

the film (DasGupta et al., 1995). Equation 30 was then used to obtain the value of the Hamaker constant, which characterizes the interfacial properties of the experimental system. Experimental results for the value of the disjoining pressure are compared with theoretical predictions in Figure 11. Considering the use of the measured curvature and the fourth power of the measured adsorbed film thickness, the agreement is very good. Although an ellipsometer was not used in these studies for the direct measurement of the adsorbed film thickness, the interpretation of interferometer results was aided by the use of both an ellipsometer and an interferometer in DasGupta et al. (1993).

The experimental setup given in Figure 12 was used by Karthikeyan et al. (1998) to study the nonisothermal CVB. Figure 13 shows a plot of the experimentally obtained temperature difference θ between the outside surface of the CVB cell and the room vs. the axial distance x for the CVB cell operating both as a CVB heat exchange and as a dry evacuated cell. The power inputs to the heater at one end of the cell and the coolers at the other end were the same in both cases. However, we see a dramatic difference between the two temperature profiles showing the effect of phase change on conductance. While the temperature profile in the dry cell resembles that of a simple fin with convective losses to the surroundings, the temperature profile in the CVB heat exchanger is more complex. In the intermediate region between the evaporator and condenser, it is almost flat showing almost no phase change with a very large effective axial conductivity. A small vapor pressure drop gives sufficient vapor flow because the vapor space is relatively large. In the evaporation region, large changes in the temperature gradient occur, thereby allowing the evaporation rate to be determined. The return liquid flow in the corners of the intermediate region is driven by the curvature and the disjoining pressure gradients. The corner radius of curvature profiles K_∞ obtained using the IAI for a slightly inclined cell are presented in Figure 14 for both cases. Additional results for the CVB are given in Karthikeyan et al. (1998) and, for other experimental designs, in DasGupta et al. (1994) and in Kim and Wayner (1996).

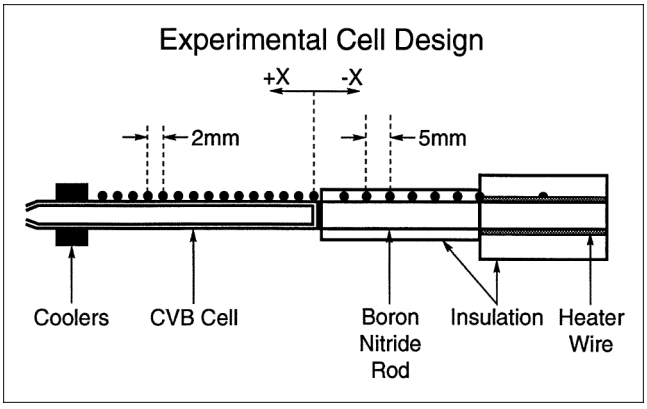

Figure 12. Experimental setup for studying the CVB.

CVB is placed on the stage of an optical microscope (not shown) with a video camera for image recording and analysis.

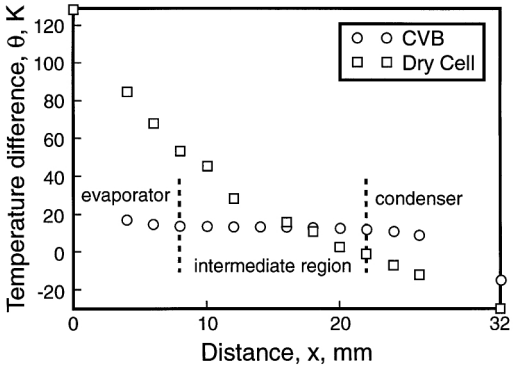

Figure 13. Temperature difference θ between the outside surface of the CVB cell and the room vs. the axial distance x for both the cell operating as a CVB heat exchanger and as a dry evacuated cell.

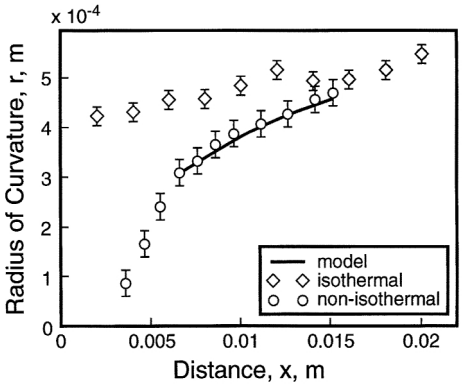

Figure 14. Corner radius of curvature profiles obtained using the IAI for both the cell operating as a CVB heat exchanger and at equilibrium.

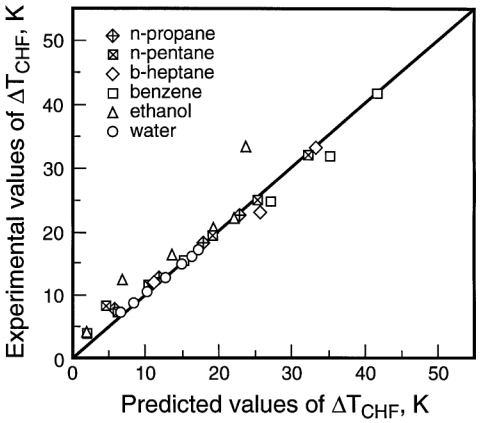

Figure 15. Comparison of experimental and predicted values of ΔT_{CHF} for polar and nonpolar fluids obtained by Reyes and Wayner (1995) using Eq. 34.

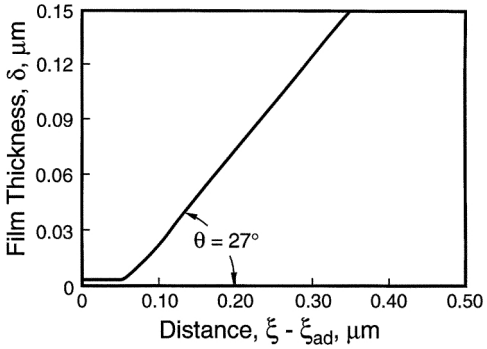

Figure 16. Meniscus thickness profile in the micro region: R114/Cu, $P_v = 2.47$ bar, $T_{out} - T_{sat} = 3.5$ K, bubble radius $r = 0.125$ mm (Stephan and Hammer, 1994).

Adsorbed film thickness at the contact line was 1 nm with $\bar{A} = 2 \times 10^{-21}$ J.

Due to the relatively large size of the above discussed CVB with an inside width of 3 mm, the system is asymmetrical in the earth's gravitational field. However, since the viscous forces are lower in thicker liquid films, the heat flux scales with the inside characteristic length. Therefore, micro heat pipes are better suited for the earth's environment and larger systems are well suited for a microgravity environment. To study the high flux axisymmetric CVB system, a microgravity experiment is planned for the year 2003. The axisymmetric CVB system is also ideal for studying the stability of evaporating thin films.

Using an extension of the above Kelvin-Clapeyron model, Reyes and Wayner (1995) obtained Eq. 34 for the superheat at the critical heat flux ΔT_{CHF}. Since the effect of the liquid-solid experimental system on adsorption at the contact line needs to be known in Eq. 34, the experimental intermolecular force for a particular system in pool boiling is characterized using the experimental measurement of the superheat at one pressure level. Then, Eq. 34 can be used to predict the value of ΔT_{CHF} at other pressures. Results are presented in Figure 15 in which the highest value of the superheat for a particular system was used to obtain the constant in Eq. 34. Exceptional agreement between predictions and experiments is obtained for the higher pressures. Using additional assumptions, Eq. 35 was obtained by Wayner (1994a) for the ΔT_{CHF} in which a calibration point is not needed. Although Eq. 35 is based on basic interfacial concepts and simpler to use, it is more approximate since the exact interfacial details for an experimental system are assumed. $\delta_o = D_s = 0.165$ nm in these studies. However, an acceptable agreement with experimental results was obtained for systems at atmospheric pressure in which the substrate surface was not excessively modified from normal (that is, normal smoothness and preparation)

$$\frac{\Delta T_{CHF} \Delta h_m \rho_1}{\sigma^{1.5} T_v} = \text{constant} \tag{34}$$

$$\frac{\Delta T_{CHF} \Delta h_m \rho_1 \delta_o}{\sigma T_v} = 0.5 \tag{35}$$

Stephan and Hammer (1994) successfully used the above interfacial models represented by Eq. 32 to evaluate the influence of meniscus curvature, adhesion forces, interfacial forces, interfacial thermal resistance, and wall thermal resistance on nucleate boiling heat transfer for the R114/Cu, $(C_2Cl_2F_4)$/Cu system. For the single bubble and microlayer presented in Figure 2, Stephan and Hammer calculated the physical details of the boiling heat-transfer process presented in Figures 16 and 17. Realistic temperature, liquid thickness and heat flux profiles were obtained and the modeling results agreed with the macroscopic experimental results. Additional examples of studies on the effect of thin film evaporation on boiling are Lay and Dhir (1995) and Sadasivan et al. (1995). In an earlier article, Stephan and Busse (1992) successfully used the same type of modeling to analyze the heat-transfer coefficient of grooved evaporator walls.

The above models predict that the slope of the meniscus interface δ' at a particular thickness should be a function of the dimensionless heat sink in the contact line region. An

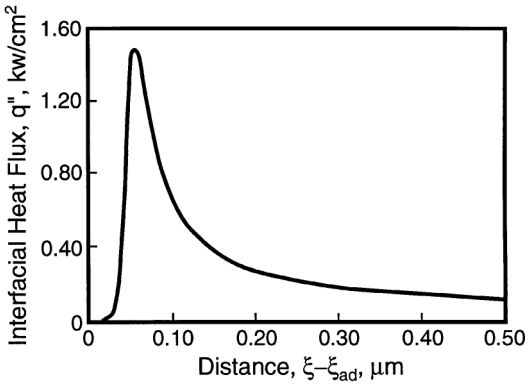

Figure 17. Interfacial heat flux distribution in the micro region: R114/Cu, $P_v = 2.47$ bar $T_{out} - T_{sat} = 3.5$ K, $r = 0.125$ mm (Stephan and Hammer, 1994).

Heat flow lines converge into the microlayer for an average input heat flux of $q''_{in} = 1901$ W/m^2.

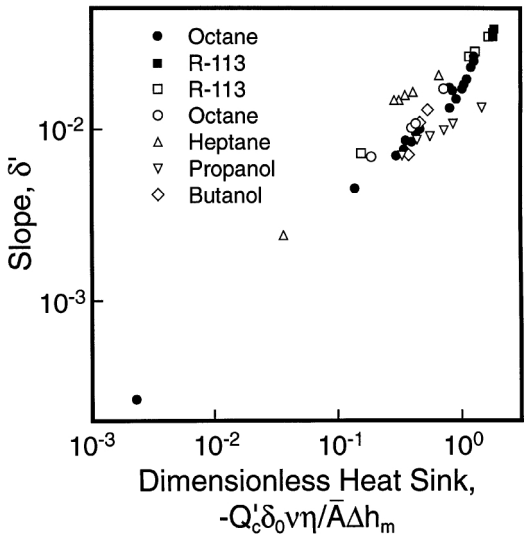

Figure 18. Meniscus slope at $\delta = 20$ nm vs. dimensionless heat sink in the contact line region (Kim and Wayner, 1996).

experimental confirmation of this prediction is presented in Figure 18. In these studies, ellipsometry was used to measure the thickness of the absorbed film δ_o at the contact line and IAI was used to measure the thickness profile. The value of the important Hamaker constant was obtained by fitting the profile data with Eq. 32.

Concluding Remarks

Theoretical and confirming experimental studies have demonstrated that models based on the disjoining pressure, capillary pressure, Kelvin, and Clapeyron concepts describe change-of-phase heat transfer and fluid flow in extremely thin liquid films. The variation of long-range intermolecular forces near interfaces profoundly affects the performance of heat exchangers. Designs need to be optimized using these concepts. Additional studies at the interfacial molecular level and the evaluation of the effects of chemical composition and stability are needed.

Acknowledgment

This material is based on work supported by the National Aeronautics and Space Administration under grant No. NAG3-1834. Any opinions, findings, and conclusions or recommendations expressed in this publication are those of the authors and do not necessarily reflect the view of NASA.

Notation

$\bar{A} = A/(6\pi)$
B = dispersion constant in Eqs. 18 and 30
E = surface energy
F = interfacial force/area, potential energy/volume
h = enthalpy/mass or volume, heat-transfer coefficient, hydrostatic distance, Planck's constant
k = thermal conductivity, Boltzmann's constant
K = curvature, parameter
m'' = interfacial mass flux
M = molecular weight
n = index of refraction
q'' = heat flux
Q = contact line heat sink
r = radius of curvature
R = gas constant
V = molar volume
x = parallel to flow direction

Greek letters

Γ = mass-flow rate per unit width of film, adsorbate per unit area
Δ = difference
δ = liquid film thickness
δ' = slope of liquid-vapor interface
δ_α = defined by Eq. 28
ϵ = dimensionless group in Eq. 32, permittivity
η = dimensionless film thickness defined in Eq. 32
θ = apparent contact angle
κ = dimensionless group in Eq. 32
λ = parameter in Eq. 29
μ = chemical potential per molecule or mole, dynamic viscosity
ν = kinematic viscosity
ξ = dimensionless position
Π = disjoining pressure
π_e = film pressure
ρ = fluid density, number density of molecules
σ = surface free energy per unit area
ϕ = dimensionless pressure difference defined in Eq. 32
Ψ = electrostatic surface potential

Subscripts and superscripts

ad = adsorbed length
CHF = critical heat flux
d = dispersion
i = interaction, induced dipole
id = ideal based on superheat only, Eq. 2
kl = defined by Eq. 6
LW = Lifshitz-van der Waals
1M = liquid per mole
l = liquid
ll = liquid-liquid
lv = liquid-vapor
m = unit mass, molecular component
o = contact line, reference, visible range
out = outside surface
p = polar
s = solid, structural component
sg = solid-gas
sl = solid-liquid
ss = solid-solid
sv = solid-vapor
slv = solid-liquid-vapor
vr = reference vapor
x = evaluated at x
$'$ = derivative
∞ = infinity, Figure 10

Literature Cited

Bangham, D. H., "The Gibbs Adsorption Equation and Adsorption on Solids," *Trans. Faraday Soc.*, **33**, 805 (1937).
Bankoff, S. G., "Dynamics and Stability of Thin Heated Liquid Films," *J. of Heat Transfer*, **112**, 538 (1990).
Bankoff, S. G., "Significant Questions in Thin Film Heat Transfer," *J. of Heat Transfer*, **116**, 10 (1994).
Carey, V. P., *Liquid-Vapor Phase-Change Phenomena: An Introduction to the Thermophysics of Vaporization and Condensation Processes in Heat Transfer Equipment*, Hemisphere Publishing Corp., Washington, DC (1992).
Churaev, N. V., "Contact Angles and Surface Forces," *Colloid J.*, **56**, 631 (1994).
Cotter, T. P., "Principles and Prospects for Micro Heat Pipes," *Proc. of 5th Int. Heat Pipe Conf.*, Tsukuba, Japan, 328 (1984).

DasGupta, S., J. A. Schonberg, and P. C. Wayner, Jr., "Investigation of an Evaporating Extended Meniscus Based on the Augmented Young-Laplace Equation," *J. Heat Transfer*, **115**, 201 (1993).
DasGupta, S., I. Y. Kim, and P. C. Wayner, Jr., "Use of the Kelvin-Clapeyron Equation to Model an Evaporating Microfilm," *J. Heat Transfer*, **116**, 1007 (1994).
DasGupta, S., J. L. Plawsky, and P. C. Wayner, Jr., "Interfacial Force Field Characterization in a Constrained Vapor Bubble Thermosyphon," *AIChE J.*, **41**, 2140 (1995).
Davis, H. T., and L. E. Scriven, "Gradient Theory of Fluid Microstructure," *J. of Statistical Physics*, **24**, 243 (1981).
Derjaguin, B. V., S. V. Nerpin, and N. V. Churayev, "Effect of Film Transfer Upon Evaporation of Liquids from Capillaries," *Bulletin Rilem No. 29*, 107 (1965).
Derjaguin, B. V., N. V. Churaev, and Y. I. Rabinovich, *Adv. in Colloid and Interface Sci.*, **28**, 197 (1988).
deFeijter, J. A., "Thermodynamics of Thin Films," *Thin Liquid Films: Fundamentals and Applications*, I. B. Ivanov, ed., Marcel Dekker, New York, p. 1 (1988).
Dzyaloskinskii, I. E., E. M. Lifshitz, and L. P. Pitaevskii, "The General Theory of van der Waals Forces," *Adv. Phys.*, **10**, 165 (1961).
Evans, R., U. Marini Bettolo Marconi, and P. Tarazona, "Fluids in Narrow Pores: Adsorption, Capillary Condensation, and Critical Points," *J. Chem. Phys.*, **84**, 2376 (1986).
Faghri, A., *Heat Pipe Science and Technology*, Taylor and Francis, Washington, DC (1995).
Fisher, L. R., and J. N. Israelachvili, "Experimental Studies on the Applicability of the Kelvin Equation to Highly Curved Concave Menisci," *J. of Colloid and Interface Sci.*, **80**, 528 (1981).
Gee, M. L., T. W. Healy, and L. R. White, "Hydrophobicity Effects in the Condensation of Water Films on Quartz," *J. of Colloid and Interface Sci.*, **140**, 450 (1990).
Gibbs, J. W., *The Scientific Papers of J. W. Gibbs, Vol. one, Thermodynamics*, Dover Publs., New York (1961).
Ha, J. M., and G. P. Peterson, "Capillary Performance of Evaporating Flow in Micro Grooves: An Analytical Approach for Very Small Tilt Angles," *J. of Heat Transfer*, **120**, 452 (1998).
Hallinan, K. P., H. C. Chebaro, S. J. Kim, and W. S. Chang, "Evaporation from an Extended Meniscus for Nonisothermal Interfacial Conditions," *J. of Thermophysics and Heat Transfer*, **8**, 709 (1994).
Holm, F. W., and S. P. Goplen, "Heat Transfer in the Meniscus Thin-Film Transition Region," *J. of Heat Transfer*, **101**, 543 (1979).
Huang, J., M. Karthikeyan, J. L. Plawsky, and P. C. Wayner, Jr., "Experimental Study and Modeling of the Effect of Low-Level Impurities on the Operation of the Constrained Vapor Bubble," *AIP Conf. Proc. 420, Part 1, Space Technol. and Appl. Int. Forum*, Albuquerque, NM, p. 446 (1998).
Israelachvili, J., *Intermolecular and Surface Forces*, 2nd ed., Academic Press, New York (1992).
Ivanov, I. B., *Thin Liquid Films: Fundamentals and Applications*, Marcel Dekker, New York (1988).
Kamotani, Y., "Evaporator Film Coefficients of Grooved Heat Pipes," *A Collection of Papers, Int. Heat Pipe Conf.*, Palo Alto, CA, AIAA, Reston, VA, p. 128 (1978).
Karthikeyan, M., J. Huang, J. Plawsky, and P. C. Wayner, Jr., "Experimental Study and Modeling of the Intermediate Section of the Nonisothermal Constrained Vapor Bubble," *J. of Heat Transfer*, **120**, 166 (1998).
Khanna, R., A. T. Jameel, and A. Sharma, "Stability and Breakup of Thin Polar Films on Coated Substrates: Relationship to Macroscopic Parameters of Wetting," *Ind. Eng. Chem. Res.*, **35**, 3081 (1996).
Khrustalev, D., and A. Faghri, "Thermal Analysis of a Micro Heat Pipe," *Heat Pipes and Capillary Pumped Loops*, A. Faghri, A. J. Juhasz, T. Mahfekey, eds., HTD-Vol. 236, ASME, New York, p. 19 (1993).
Khrustalev, D., and A. Faghri, "Heat Transfer During Evaporation on Capillary Grooved Structures of Heat Pipes," *J. of Heat Transfer*, **117**, 740 (1995).
Kim, I-Y., and P. C. Wayner, Jr., "The Shape of an Evaporating Completely Wetting Extended Meniscus," *AIAA J. of Thermophy. and Heat Transfer*, **10**, 320 (1996).
Kistler, S. F., "Hydrodynamics of Wetting," *Wettability*, J. C. Berg, ed., Marcel Dekker, New York (1993).
Klein, J., and E. Kumacheva, "Confinement-Induced Phase Transitions in Simple Liquids," *Science*, **269**, 816 (1995).
Knudstrup, T. G., I. A. Bitsanis, and G. B. Westermann-Clark, "Pressure-Driven Flow Experiments in Molecularly Narrow, Straight Pores of Molecular Dimensions in Mica," *Langmuir*, **11**, 893 (1995).
Koplik, J., "Continuum Deductions from Molecular Hydrodynamics," *Annu. Rev. Fluid Mech.*, **27**, 257 (1995).
Lay, J. H., and V. K. Dhir, "Shape of a Vapor Stem During Nucleate Boiling of Saturated Liquids," *J. of Heat Transfer*, **117**, 394 (1995).
Maa, J. R., "The Role of Interfaces in Heat Transfer Processes," *Adv. in Colloids and Interface Sci.*, **18**, 227 (1983).
Mantel, M., and J. P. Wightman, "Influence of the Surface Chemistry on the Wettability of Stainless Steel," *Surface and Interface Anal.*, **21**, 595 (1994).
Mitrovic, J., "The Flow and Heat Transfer in the Wedge-Shaped Liquid Film Formed During the Growth of a Vapor Bubble," *Int. J. Heat Mass Transfer*, **41**, 1771 (1998).
Morris, S. J. S., and V. Moreno, "Systematic Analysis of an Evaporating Wetting Meniscus on a Smooth Surface," HTD-Vol. 349, ASME Proc. of the 32nd National Heat Transfer Conf., Vol. 11, ASME (1997).
Morris, S. J. S., "A Phenomenological Treatment of an Evaporating, Perfectly-Wetting Meniscus," *J. of Fluid Mechanics*, in press (1999).
Moosman, S., and G. M. Homsy, "Evaporating Menisci of Wetting Fluids," *J. Colloid and Interface Sci.*, **73**, 212 (1980).
Oron, A., S. H. Davis, and S. G. Bankoff, "Long-Scale Evolution of Thin Liquid Films," *Rev. of Modern Physics*, **69**, 931 (1997).
Parks, C. J., and P. C. Wayner, Jr., "Surface Shear Near the Contact Line of a Binary Curved Thin Film," *AIChE J.*, **33**, 1 (1987).
Parsegian, V. A., G. H. Weiss, and M. E. Schraeder, "Macroscopic Continuum Model of Influence of Hydrocarbon Contamination on Forces Causing Wetting of Gold by Water," *J. Colloid and Interface Science*, **61**, 356 (1977).
Potash, M., Jr., and P. C. Wayner, Jr., "Evaporation from a Two-Dimensional Extended Meniscus," *Int. J. Heat Mass Transfer*, **15**, 1851 (1972).
Raiff, R. J., and P. C. Wayner, Jr., "Evaporation from a Porous Flow Control Element on a Porous Heat Source," *Int. J. Heat Mass Transfer*, **16**, 1919 (1973).
Read, A. D., and J. A. Kitchener, *J. Colloid and Interface Sci.*, **30**, 391 (1969).
Reyes, R., and P. C. Wayner, Jr., "An Adsorption Model for the Superheat at the Critical Heat Flux," *J. of Heat Transfer*, **117**, 779 (1995).
Reyes, R., and P. C. Wayner, Jr., "A Kelvin-Clapeyron Adsorption Model for Spreading on a Heated Plate," *J. of Heat Transfer*, **118**, 822 (1996).
Rowlinson, J. S., Translation of J. D. van der Waals' "The Thermodynamics Theory of Capillarity Under the Hypothesis of a Continuous Variation of Density," *J. of Statistical Phys.*, **20**, 197 (1979).
Sadasivan, P., C. Unal, and R. Nelson, "Perspective: Issues in CHF Modeling—The Need for New Experiments," *J. of Heat Transfer*, **117**, 558 (1995).
Sharma, A., "Equilibrium and Dynamics of Evaporating or Condensing Thin Film Domains: Thin Film Stability and Heterogeneous Nucleation," *Langmuir*, **14**, 4915 (1998).
Sharma, A., "Equilibrium Contact Angles and Film Thicknesses in the Apolar and Polar Systems: Role of Intermolecular Interactions in Coexistence of Drops with Thin Films," *Langmuir*, **9**, 3580 (1993).
Stephan, P., and C. A. Busse, "Analysis of the Heat Transfer Coefficient of Grooved Heat Pipe Evaporator Walls," *Int. J. Heat Mass Transfer*, **35**, 383 (1992).
Stephan, P., and J. Hammer, "A New Model for Nucleate Boiling Heat Transfer," *Warme- und Stoffubertragung*, **30**, 119 (1994).
Swanson, L. W., and G. C. Herdt, "Model of the Evaporating Meniscus in a Capillary Tube," *J. of Heat Transfer*, **114**, 434 (1992).
Swanson, L. W., and G. P. Peterson, "The Interfacial Thermodynamics of Micro Heat Pipes," *J. of Heat Transfer*, **117**, 195 (1995).
Truong, J. G., and P. C. Wayner, Jr., "Effects of Capillary and van der Waals Dispersion Forces on the Equilibrium Profile of a Wetting Liquid: Theory and Experiment," *J. Chem. Phys.*, **87**, 4180 (1987).
van Oss, C. J., *Interfacial Forces in Aqueous Media*, Marcel Dekker, New York (1994).

Vigil, G., Z. Xu, S. Steinberg, and J. Israelachvili, "Interactions of Silica Surfaces," *J. of Colloid and Interface Sci.*, **165**, 367 (1994).
Wayner, P. C., Jr., Y. K. Kao, and L. V. LaCroix, "The Interline Heat Transfer Coefficient of an Evaporating Wetting Film," *Int. J. Heat Mass Transfer*, **19**, 487 (1976).
Wayner, P. C., Jr., "The Effect of the London-van der Waals Dispersion Force on Interline Heat Transfer," *J. of Heat Transfer*, **100**, 155 (1978).
Wayner, P. C., Jr., "The Interfacial Profile in the Contact Line Region and the Young-Dupré Equation," *J. Colloid and Interface Sci.*, **88**, 294 (1982).
Wayner, P. C., Jr., C. Y. Tung, M. Tirumala, and J. H. Yang, "Experimental Study of Evaporation in the Contact Line Region of a Thin Film of Hexane," *J. of Heat Transfer*, **107**, 182 (1985).
Wayner, P. C., Jr., "The Effect of Interfacial Mass Transport on Flow in Thin Liquid Films," *Colloids and Surfaces*, **52**, 71 (1991).
Wayner, P. C., Jr., "Thermal and Mechanical Effects in the Spreading of a Liquid Film Due to a Change in the Apparent Finite Contact Angle," *J. of Heat Transfer*, **116**, 938 (1994a).
Wayner, P. C., Jr., "Mechanical and Thermal Effects in the Forced Spreading of a Liquid Film with a Finite Contact Angle," *Colloids and Surfaces A*, **89**, 89 (1994b).
Wu, D., and G. P. Peterson, "Investigation of the Transient Characteristics of a Micro Heat Pipe," *J. Thermophys.*, **5**, 129 (1991).

Manuscript received Mar. 29, 1999, and revision received June 28, 1999.